BBA - Molecular Basis of Disease 1865 (2019) 165526

Contents lists available at ScienceDirect

BBA - Molecular Basis of Disease

journal homepage: www.elsevier.com/locate/bbadis

Vibrational spectroscopy-based quantification of liver steatosis

E. Szafraniec[a,b], S. Tott[a,b], E. Kus[b], D. Augustynska[b], A. Jasztal[b], A. Filipek[a], S. Chlopicki[b], M. Baranska[a,b,*]

[a] Faculty of Chemistry, Jagiellonian University, Gronostajowa 2, 30-387 Krakow, Poland
[b] Jagiellonian Centre for Experimental Therapeutics (JCET), Jagiellonian University, Bobrzynskiego 14, 30-348 Krakow, Poland

ARTICLE INFO

Keywords:
Liver steatosis
Lipids
Vibrational spectroscopy
Oil red O staining

ABSTRACT

The liver plays a central role in lipid metabolism, and abnormal lipid accumulation in the liver is a key feature of Non-Alcoholic Fatty Liver Disease. In experimental studies, quantification of liver steatosis is commonly based on lipids staining or biochemical analysis. Here, we present a spectroscopic approach for quantitative analysis of the lipid content in the freeze-dried liver. The method is based on vibrational spectroscopy (Raman and infrared) measurements applied for Partial Least Squares (PLS) regression modeling. The obtained PLS models show a good correlation of the spectroscopic data with the reference histological evaluation of steatosis based on Oil Red O (ORO)-stained images of liver cross sections. Vibrational spectroscopy with PLS-based modeling described here represents a useful approach for the fast assessment of the liver steatosis in a small sample of freeze-dried liver tissue. In conclusion, our work demonstrates the easy-to-use method that can be applied in laboratory routine as a beneficial alternative to the established ORO staining.

1. Introduction

Non-Alcoholic Fatty Liver Disease (NAFLD), is the most common chronic liver disease, with increasing prevalence worldwide [1–3]. It starts from an excess of hepatic lipid accumulation (isolated steatosis) that may progress to advanced stages of non-alcoholic steatohepatitis and fibrosis increasing the risk of cirrhosis and hepatocellular carcinoma [4–10]. Furthermore, NAFLD is supposed to be involved in the pathogenesis of cardiovascular disease [11].

Despite the central role of NAFLD in various diseases, there is still no easy-to-use gold-standard method for precise total lipid content quantification in the liver [12]. In experimental studies, one of the most reliable techniques for this purpose that is routinely used to quantify liver steatosis is a staining based on lysochrome, Oil Red O (ORO) [13,14]. A hydrophobic dye used in this technique, with the absorption maximum at 518 nm, labels the neutral lipids (tri- and diacylglycerols) and cholesteryl esters in cells and tissues [15]. After staining, the amount of lipids is estimated with a simple calculation of stained area on the visible images, or as a ratio of stained to whole tissue section area [13]. ORO staining is still a gold-standard method, however, it has some limitations [12]. First of all, ORO staining is a time-consuming technique because it requires a complex sample preparation. Moreover, there is a restraint for samples for which it can be applied, e.g., alcohol-fixed or paraffin-embedded tissues cannot be used due to extraction of most lipids in these procedures. Finally, ORO staining does not give any analytical information about different lipid species in the tissue and it can be used solely for the quantification of neutral lipids because it does not label polar lipids [16]. These limitations of ORO staining prompted us to look for an alternative method.

Numerous studies show the capability of vibrational spectroscopy for biomedical applications because it can provide rapid and precise information on biochemical content of samples. Non-destructiveness and label-free measurements are the additional advantages of vibrational spectroscopy techniques. Raman as well as IR spectroscopy have been successfully applied for various studies on liver tissue and cells, including cancer detection [17,18], evaluation of liver fibrosis [19,20] and liver steatosis [21–23].

Lipids, due to their characteristic spectroscopic features, can be easily detected with the use of Raman and IR, and both techniques have repeatedly proved to be perfectly suited for the analysis of lipid tissue contents [24,25]. Spectral signals of lipids originate mostly from the hydrocarbon chain vibrations. Characteristic bands of lipids can be assigned to CH_2/CH_3 scissoring and twisting vibrations (deformations) in the range of 1500–1300 cm^{-1}, and C—C stretching vibrations observed in the range of 1200–1050 cm^{-1}. In addition, C—H stretching modes give rise to a very characteristic and intense group of bands in the higher wavenumber range (~3100–2800 cm^{-1}) [26]. The detailed investigation of the nature of lipid compounds of the sample is also

* Corresponding author at: Faculty of Chemistry, Jagiellonian University, Gronostajowa 2, 30-387 Krakow, Poland.
E-mail address: baranska@chemia.uj.edu.pl (M. Baranska).

https://doi.org/10.1016/j.bbadis.2019.08.002
Received 28 May 2019; Received in revised form 31 July 2019; Accepted 5 August 2019
Available online 06 August 2019

possible because information on, e.g., the presence of unsaturated bonds or cholesterol and its esters is easy to gain from both Raman and IR spectra. However, the quantitative analysis of tissue with the use of Raman or IR spectroscopies usually requires a reference method to be applied, e.g., chromatography [27,28] or tissue staining [29].

Previously, few reports addressed the quantification of liver steatosis using Raman probes [30,31], IR imaging [29], Coherent Anti-Stokes Raman Scattering [32] and Stimulated Raman Scattering [33] microscopies. The latter seem to fit perfectly to this application because of their speed, high chemical specificity and label-free manner, however, they are not very cost-effective [34]. Here, we decided to evaluate the use of basic FT-Raman and compact benchtop ATR-FT-IR spectrometers for rapid quantification of lipid accumulation in liver tissue. For this purpose, spectroscopic data were compared with results from the ORO staining by applying Partial Least Squares (PLS) regression, a method commonly used to model the relationship between two data matrices [27,35,36]. A previous similar study showed that FT-IR imaging of liver tissue cross sections provides comparable information as the ORO-based method with no need for labeling [29]. Here, however, we aimed to simplify the protocol further, utilizing the single-point measurement from the freeze-dried and homogenized samples, instead of imaging tissue cross sections. This approach does not require the precise cutting of the tissue followed by time-consuming imaging and analysis. Our results showed that through application of two conventional techniques, the gold-standard ORO staining and Raman or IR spectroscopy, it is possible to build a reliable mathematical model based on PLS regression that can be further used for the quantification of liver steatosis based on a single spectrum measurement.

2. Material and methods

2.1. Animals and experimental design

Six-week-old, male C57BL/6J mice were fed on the control (AIN-93G) or high-fat diet (HFD; 60 kcal% of fat with 1% cholesterol) (Research Diets, USA) for 0, 4 and 8 weeks. After feeding time, 10 mice at each time point were anesthetized with an intraperitoneal injection of ketamine (100 mg/kg of body weight) and xylazine (10 mg/kg of body weight) and the liver was excised. Then, three liver lobes (left, medial, and right) were isolated and prepared for histological staining and spectroscopic measurements.

2.2. Oil Red O staining

Liver samples were fixed in 4% buffered formalin (Chempur, Piekary Slaskie, Poland). Samples were embedded in Optimal Cutting Temperature (OCT) medium (Bio Optica, Milano, Italy) and stored at −80 °C. OCT embedded, 7 μm sections were stained with ORO (Sigma-Aldrich, St. Louis, MO, USA) for fat content examination. Randomly chosen areas of tissue sections were photographed using an Olympus BX51 light microscope (Tokyo, Japan) equipped with Olympus UPlan Apo 20× objective. The ORO-stained sections were analyzed for lipid content by the Columbus Image Data Storage and Analysis System (PerkinElmer, USA) adapted for ORO-stained sections algorithm and expressed as % of liver tissue area stained positively for lipids. Because of the heterogeneity of the liver tissue, this procedure was performed for three different lobes: left, right, and medial, collecting at least 10 images per lobe, in order to acquire representative information for each lobe.

2.3. Spectroscopic measurements and spectra preprocessing

For spectroscopic measurements, approximately 100 mg of a sample taken from three chosen lobes was collected. All samples were weighed and then freeze-dried for 24 h using FreeZone® freeze-dryer (LABCONCO). Then samples were stored at 4 °C. Before measurements, all samples were ground in a mortar to obtain a homogeneous powder.

Raman measurements were performed using the MultiRam FT-Raman spectrometer (Bruker, Ettlingen, Germany) equipped with 1064 nm Nd:YAG laser and a germanium detector cooled with liquid nitrogen. The power of the laser was adjusted to 200 mW. 256 scans were accumulated per spectrum and the spectral resolution was set to 8 cm^{-1}. For every sample, five spectra were measured. Spectra preprocessing was executed in the OPUS (Bruker, MA, USA) software. All spectra were smoothed with the use of the Savitzky–Golay algorithm (nine smoothing points). In the next step, the baseline was corrected with the use of concave rubber band correction (15 repeats). After removing outlier spectra (with low signal to noise ratio), the average spectrum from every sample was calculated.

Alpha Bruker spectrometer was used to collect the ATR-FT-IR spectra. Sixteen scans were accumulated per spectrum for samples and 32 scans for background measurements. For every sample, five spectra were measured. The spectral resolution was set to 4 cm^{-1}. Prior to data analysis, the data preprocessing using OPUS software was applied, including extended ATR correction (diamond, 1 reflection) and normalization (vector normalization in range of 1800–1000 cm^{-1}). The spectra were derivatised (second derivative) with the use of the Savitzky–Golay algorithm (17 smoothing points). This was done to resolve nearby lying bands in the original spectrum and precisely identify them. All applied algorithms are implemented in the Opus software.

2.4. Partial Least Squares regression

The PLS regression was used here to determine the property Y of a system from an experimentally observable X, whereby X and Y are correlated by a calibration function: $\vec{Y} = X \cdot \vec{b}$. The vector Y consists of the component values as determined by the reference measurements (here the ORO staining). The row vectors of the matrix X are formed from the calibration spectra (here the Raman/infrared spectra of the liver sample). The aim is to determine the vector b. When the b is known, the prediction of unknown values for Y can be performed. In general, the PLS analysis shows the correlation between the component values and the spectral intensities. A description of the mathematical algorithm that is involved in the PLS regression analysis of the data is provided with more details in the literature [37,38].

A well-constructed PLS model can be used to predict the values of the parameters describing the level of steatosis. In our case, the reference data from ORO staining provided the information on the percentage of the tissue's area containing lipids. The first step was to calculate the correlation between the averaged spectra collected for each animal and three liver lobes (right, left, medial) with the ORO data. Moreover, models based on FT-Raman and ATR-FT-IR spectroscopies were compared to verify their efficiency in predicting the level of hepatic steatosis. PLS models were constructed for samples taken from the three liver lobes (left, medial and right) and calculated separately for each lobe, as well as for the sum of them. For that purpose, the spectroscopic and ORO data were divided into a “training” data set for which the PLS model was built, and a “test” data set that was used for estimation of the liver steatosis.

For that purpose, the spectra preprocessed as described in Section 2.3 were used for the PLS model construction. The dataset (n = 30) was defined as the averaged spectra representing each animal and corresponding to the level of steatosis (the percentage of tissue stained with ORO). The data were divided into a training set (n = 20) and test set (n = 10), each containing samples with varying degrees of steatosis. The PLS analysis was performed within the ranges of 2840–3040 cm^{-1} (Raman spectroscopy, RS) and 1590–1780 cm^{-1} (IR spectroscopy, IR) for an optimal correlation with the level of steatosis. In the case of IR measurements, the second derivatives of the spectra were used for analysis. For calculations and presentation of the results, the OPUS and the Origin 2018 software (OriginLab Corporation, MA, USA) were used.

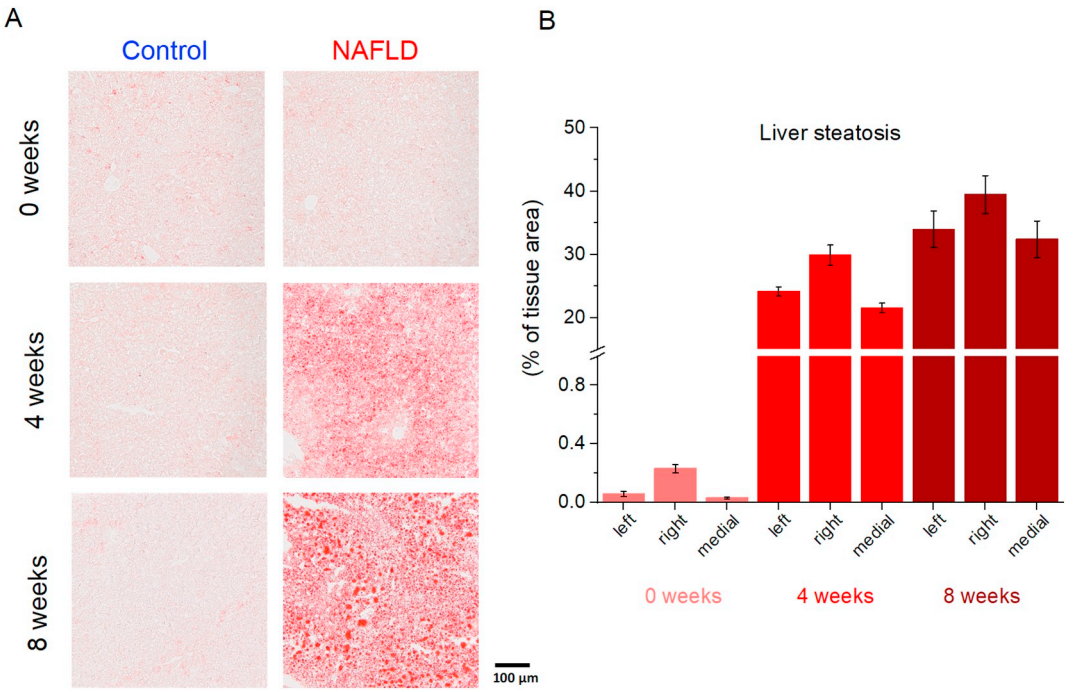

Fig. 1. Oil red O-stained section of liver taken from the left liver lobe of mice fed for 0, 4 and 8 weeks standard AIN-93G diet and HFD diet (A). Semi-automatic quantitative analysis of ORO-stained liver fat content in NAFLD mice using the Columbus software for three different liver lobes (left, right, medial) presented for NAFLD samples.

3. Results and discussion

3.1. Assessment of liver steatosis by ORO staining

As shown in Fig. 1, the HFD induced micro and macrovesicular steatosis in the mice. An automatic quantitative analysis of liver fat content using the Columbus software was applied to image the sections of stained tissues. It revealed a significant increase in the liver steatosis compared with the control because the lipids occupied 20–30% of the tissue area after 4 weeks of HFD feeding and up to 40% after 8 weeks of HFD feeding. Furthermore, for each experimental time point (0, 4 and 8 weeks) the trend of the highest fat content in the right lobe was observed as compared with other lobes.

3.2. Assessment of liver steatosis by spectroscopic analysis

The spectroscopic characterization of the lipid content was performed on freeze-dried samples of exactly the same livers used for ORO staining. Because liver steatosis is heterogeneous between the lobes as well as inside the lobes [39], to get average information on the level of steatosis, freeze-drying and mechanical homogenization of the liver were performed. Complementary FT-Raman (with 1064 nm laser) and ATR-IR techniques were implemented.

Liver samples have been widely explored using RS [24,31–32] and IR [33–35] and its spectral characteristics are well described. In brief, the RS spectrum of liver tissue is composed of bands characteristic for proteins at 1658 (amide I) and 1005 cm^{-1} (phenylalanine), and lipids at 2854 (C—H stretch), 1658 (C=C stretching), 1444 (CH_2, CH_3 deformation), 1305 (–CH_2 deformation) or 1266 cm^{-1} (=CH_2 deformation) and lipid esters at 1754 cm^{-1} (Fig. 2). In the IR spectrum of liver tissue, these bands were present at similar positions, however, band at 1545 cm^{-1} (amide II, proteins) is hardly seen in the RS spectrum, as well as the characteristic set of bands attributed to glycogen at 1152, 1080, 1030 cm^{-1} (Fig. 2). On the other hand, vitamin A signals were observed in the RS spectrum at 1590, 1205 and 1158 cm^{-1} (although much weaker, due to lack of resonance, which can be observed, e.g., when 532 nm laser is used), while they are not present in the IR spectrum. A detailed list of Raman and IR bands detected at liver samples can be found in Table 1 together with their assignment.

The RS and IR spectra of three different liver lobes (right, left and medial) are presented together (Fig. 2). The right lobe is characterized by a slightly higher intensity of lipid-specific bands, indicating higher content of lipids in this lobe in comparison to the left and medial ones, which is in agreement with results obtained from ORO staining (see Fig. 1).

3.3. Analysis of NAFLD progression based on vibrational spectra compared with ORO staining

Vibrational spectra of the right liver lobe collected for each experimental time point from NAFLD and the control group are shown in Fig. 3. In the case of Raman spectra, the increase of the overall lipid content, as a result of HFD was manifested by an increase of the intensity of lipid bands in the high wavenumber region at 2895 and 2854 cm^{-1}, as well as in the low wavenumber spectral range at 1754 and 1305 cm^{-1}. This increased intensity of lipid Raman bands is observed in comparison to control spectra, however, also when spectra from NAFLD animals after 0, 4 and 8 weeks of HFD feeding were compared (Fig. 3). On the other hand, bands at 3015, 1658 and 1266 cm^{-1} did not exhibit a change in the intensity, which suggests that the increase of lipid content mainly concerns saturated lipids. In addition, the decrease of vitamin A marker band at 1590 cm^{-1} was observed for NAFLD samples in comparison to control, which is in agreement with previous research [21,31]. Infrared spectra exhibited a similar increase of intensity of lipid-originated bands observed at 2930, 2854, 1745 and 1464 cm^{-1} in comparison to control samples. Notably, the band that strongly increased together with the duration of HFD feeding is the band at 1745 cm^{-1} attributed to lipid esters (C=O bond stretching), which indicates an increase of triacylglycerols (TAGs) content in the liver tissue during the progression of NAFLD.

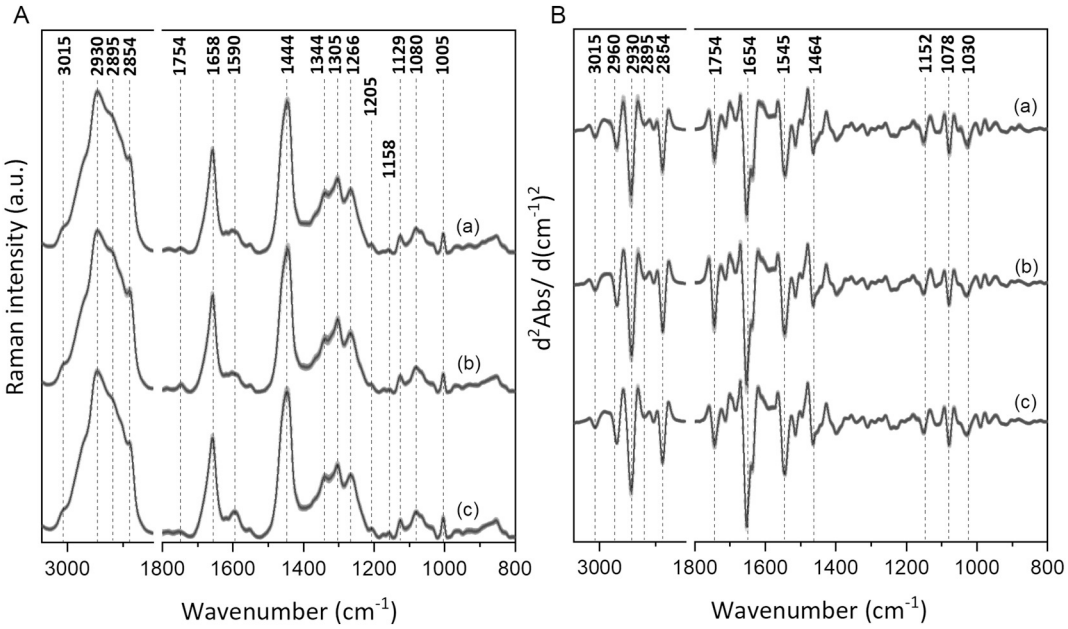

Fig. 2. Raman spectra (A) and second derivatives of infrared (B) spectra of the liver tissue samples (freeze-dried) taken from different liver lobes: (a) left, (b) right, and (c) medial. Spectra are presented with a standard error (shaded area) and offset for clarity.

Table 1
Assignment of the bands identified by the FT-Raman (RS) and FT-IR (IR) spectra.

Band position [cm^{-1}]	Assignment
3015 (RS, IR)	ν(=C–H), lipids
2960 (IR)	ν_{as}(C—H) –CH_3, lipids, proteins
2930 (RS, IR)	ν_s(C—H) –CH_3, lipids, proteins
2895 (RS)	ν_s(C—H) –CH_2, lipids, proteins
2854 (RS, IR)	ν_s(C—H) –CH_2, lipids, proteins
1754 (RS, IR)	ν(C=O), lipid esters
1658 (RS)	ν(C=C)/Amide I, lipids, proteins
1654 (IR)	Amide I, proteins
1590 (RS)	ν(C=C), vitamin A
1545 (IR)	δ(N—H) + ν(C—N) (amide II), proteins
1515 (IR)	ring ν(C—C) of Tyr residues, tyrosine proteins
1464 (IR)	δ(CH_2), lipids, proteins
1444 (RS)	δ(CH_2, CH_3), lipids, proteins
1344 (RS)	δ(CH_2), proteins
1305 (RS)	δ(CH_2), lipids
1266 (RS)	δ(=CH)/Amide III, lipids, proteins
1205 (RS)	ν(C—C), vitamin A
1158 (RS)	ν(C—C), vitamin A
1152 (IR)	ν(C—O), glycogen
1129 (RS)	ν(C_α–N), heme
1080 (RS)	ν(C—C) trans (acyl backbone), lipids
1078 (IR)	ν(C—C), glycogen
1030 (IR)	δ(C–O–H), glycogen
1005 (RS)	Symmetric ring breathing, phenylalanine

ν_s-symmetric stretching, ν_{as}-asymmetric stretching, δ-deformation.

3.4. Correlation between spectroscopic and ORO-staining data

The results provided by FT-Raman spectroscopy showed a very good correlation with the ORO staining, especially within the spectral range between 2840 cm^{-1} and 3040 cm^{-1}, where several bands characteristic for lipid molecules are observed, i.e., CH_2 symmetric stretching at 2854 cm^{-1}, CH_2 asymmetric stretching at 2930 cm^{-1} and =CH stretching at 3015 cm^{-1} (see Table 1). In the case of IR spectra, the best correlation with ORO staining was found for the spectral range between 1590 cm^{-1} and 1780 cm^{-1}, where the band at 1745 cm^{-1}, attributed to TAGs (ester C=O stretching), is observed. When the PLS model was built using data originating from the same lobe, the best correlation was obtained for the left lobe, both for the Raman spectroscopy (R^2 = 0.972) and IR spectroscopy (R^2 = 0.935, see Table 2). As mentioned earlier, the level of liver steatosis is known to vary between the lobes, and it was previously reported that the left lobe provides the best correlation between Raman data and histological evaluation [30]. The exemplary validation results for the left lobe are presented in Fig. 4. The comparison of the two vibrational techniques showed that both Raman and IR can be applied for the evaluation of liver steatosis.

Because we aimed to develop an easy-to-use method for quantification of liver steatosis, we decided to check if the model built for one lobe can be successfully applied when the spectra are obtained for a random part of the liver. Therefore, we used models to build for each lobe separately (left, medial, right) and tested for Raman spectra measured for different lobes, e.g., left–medial, left–right, right–medial. The result of this test is presented in Table 3. The calculations showed that PLS models provide very good prediction regardless of which liver lobe of the sample was taken. The lowest value of R^2 was obtained, as expected, for the right lobe. However, our results indicate that differences in correlation for different liver lobes are very small, therefore we postulate that any liver lobe can be used for such a PLS model.

4. Conclusions

The gold-standard method in liver steatosis studies, the ORO staining, is usually applied for a quantitative determination of the lipid content in histological samples. Here, we present an alternative approach enabling rapid and accurate determination of lipids in the liver using vibrational spectroscopy methods and freeze-dried, homogenized liver samples.

We showed that the PLS method correlating spectroscopic and ORO-staining data allows one to gain information about the level of steatosis in the liver tissue of NAFLD mice model. Spectroscopic measurements of homogenized tissue provided information of an average lipids' content, being relatively independent of the section of the part of the organ taken for analysis. Therefore, heterogeneity in a lipid's distribution in the tissue does not significantly affect the results. Utilizing two spectroscopic methods, for both FT-Raman and ATR-FT-IR we obtained PLS models of high quality, up to R^2 = 0.972 (FT-Raman) and R^2 = 0.953 (ATR-FT-IR). Altogether, both spectroscopic techniques can be considered equally effective in determining the level of steatosis in the liver

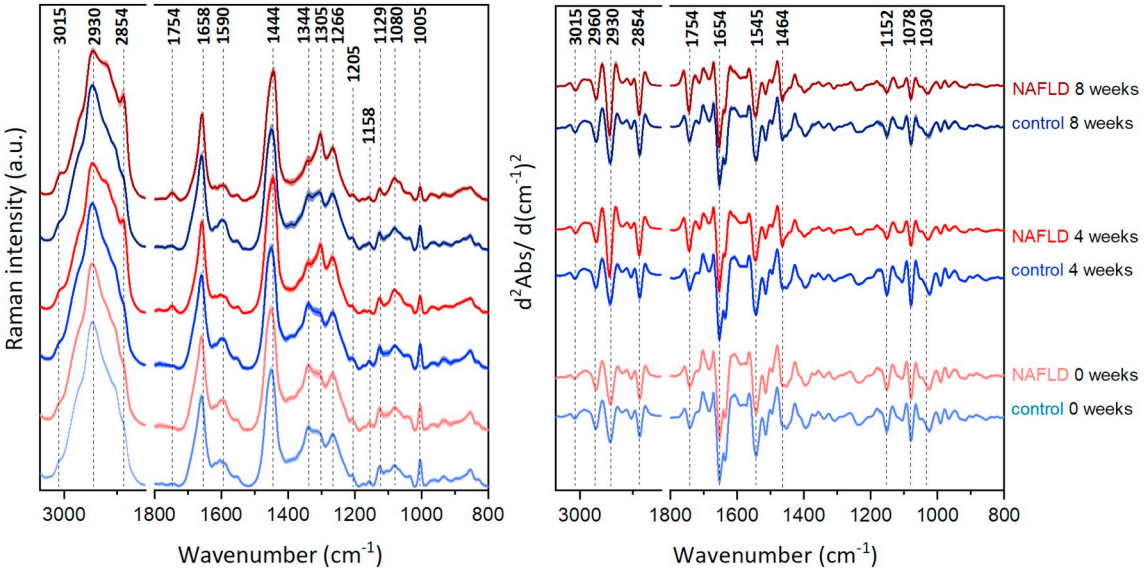

Fig. 3. Raman spectra (left) and second derivatives of infrared (right) spectra of left liver lobe taken from mice fed for 0, 4, and 8 weeks standard AIN-3G diet (Control) and HFD + 1% cholesterol (NAFLD). Spectra are presented with a standard error (shaded area) and offset for clarity.

Table 2
Values of the coefficient of determination, R^2, and the Root Mean Square Error of Prediction, *RMSEP*, describing the correlation between FT-Raman or ATR-FT-IR spectra and ORO-staining results; applied spectral ranges for Raman and IR spectra were 2840–3040 cm^{-1} and 1590–1780 cm^{-1}, respectively.

Lobe	FT-Raman spectroscopy		ATR-FT-IR spectroscopy	
	R^2	*RMSEP*	R^2	*RMSEP*
Sum	0.970	2.3	0.935	3.4
Left	0.972	2.1	0.953	2.8
Medial	0.959	2.5	0.922	3.3
Right	0.949	3.2	0.908	4.3

tissue sample, and hence the level of liver steatosis.

Transparency document

The Transparency document associated with this article can be found, in online version.

Table 3
Correlation between the Oil red O staining results (stained area/tissue area, %) and Raman spectra for samples taken from different parts of the liver: left lobe (L), median lobe (M) and right lobe (R). Coefficient of determination, R^2 (top) and Root Mean Square Error of Prediction, *RMSEP* are shown (bottom). PLS models were based on Raman spectra in the range of 2840–3040 cm^{-1}. Correlation parameters obtained for the same lobe are in bold.

RS	ORO		
	L	M	R
L	**0.972**	0.981	0.977
	2.1	1.4	2.6
M	0.992	**0.959**	0.981
	1.3	**2.5**	2.0
R	0.874	0.992	**0.949**
	4.7	0.9	**3.2**

Acknowledgments

This work was supported by the National Science Centre Poland, grant Symfonia (ID: UMO-2015/16/W/NZ4/00070). ESz acknowledges the grant Etiuda (ID: UMO-2018/28/T/ST4/00216).

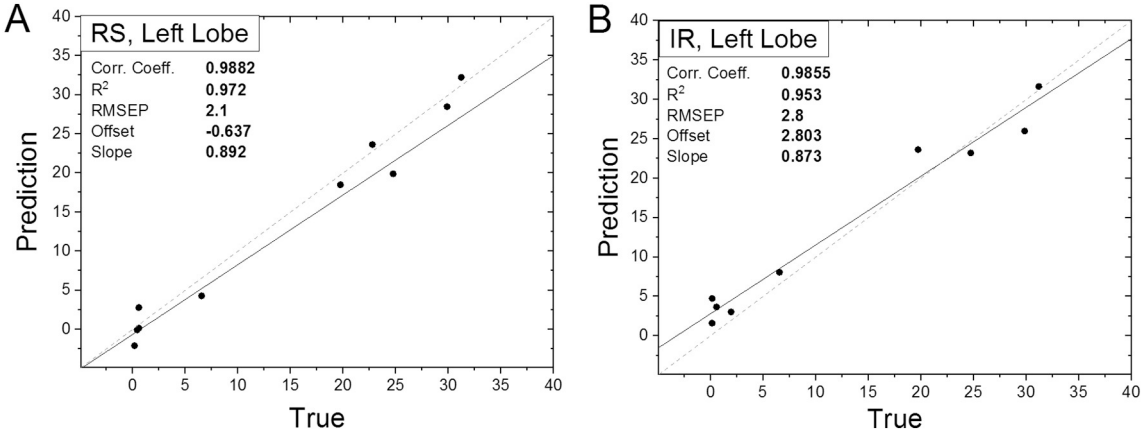

Fig. 4. Validation results for the PLS models calculated on the basis of the ORO-staining results and FT-Raman spectra (A); ATR-FT-IR spectra (B). The plots present dependences between predicted by the models and true values of the area percentage of the tissue containing lipids for the left lobe of the liver.

References

[1] Z.M. Younossi, M. Stepanova, M. Afendy, Y. Fang, Y. Younossi, H. Mir, M. Srishord, Changes in the prevalence of the most common causes of chronic liver diseases in the United States from 1988 to 2008, Clin. Gastroenterol. Hepatol. 9 (2011) 524–530.e1, https://doi.org/10.1016/j.cgh.2011.03.020.

[2] M. Sayiner, A. Koenig, L. Henry, Z.M. Younossi, Epidemiology of nonalcoholic fatty liver disease and nonalcoholic steatohepatitis in the United States and the rest of the world, Clin. Liver Dis. 20 (2016) 205–214, https://doi.org/10.1016/j.cld.2015.10.001.

[3] Y. Fazel, A.B. Koenig, M. Sayiner, Z.D. Goodman, Z.M. Younossi, Epidemiology and natural history of non-alcoholic fatty liver disease, Metab. Clin. Exp. 65 (2016) 1017–1025, https://doi.org/10.1016/j.metabol.2016.01.012.

[4] Q. Liu, S. Bengmark, S. Qu, The role of hepatic fat accumulation in pathogenesis of non-alcoholic fatty liver disease (NAFLD), Lipids Health Dis. 9 (2010) 42, https://doi.org/10.1186/1476-511X-9-42.

[5] D.M. Erion, H.-J. Park, H.-Y. Lee, The role of lipids in the pathogenesis and treatment of type 2 diabetes and associated co-morbidities, BMB Rep. 49 (2016) 139–148, https://doi.org/10.5483/BMBRep.2016.49.3.268.

[6] C.E. Hagberg, A. Mehlem, A. Falkevall, L. Muhl, B.C. Fam, H. Ortsäter, P. Scotney, D. Nyqvist, E. Samén, L. Lu, S. Stone-Elander, J. Proietto, S. Andrikopoulos, Å. Sjöholm, A. Nash, U. Eriksson, Targeting VEGF-B as a novel treatment for insulin resistance and type 2 diabetes, Nature. 490 (2012) 426–430, https://doi.org/10.1038/nature11464.

[7] D.H. Ipsen, J. Lykkesfeldt, P. Tveden-Nyborg, Molecular mechanisms of hepatic lipid accumulation in non-alcoholic fatty liver disease, Cell. Mol. Life Sci. 75 (2018) 3313–3327, https://doi.org/10.1007/s00018-018-2860-6.

[8] F.M. Perla, M. Prelati, M. Lavorato, D. Visicchio, C. Anania, The role of lipid and lipoprotein metabolism in non-alcoholic fatty liver disease, Children. 4 (2017) 46, https://doi.org/10.3390/children4060046.

[9] P. Mirmiran, Z. Bahadoran, F. Azizi, Lipid accumulation product is associated with insulin resistance, lipid peroxidation, and systemic inflammation in type 2 diabetic patients, Endocrinol. Metab. 29 (2014) 443–449, https://doi.org/10.3803/EnM.2014.29.4.443.

[10] M.-S. Kwak, D. Kim, Non-alcoholic fatty liver disease and lifestyle modifications, focusing on physical activity, Korean J. Intern. Med. 33 (2018) 64–74, https://doi.org/10.3904/kjim.2017.343.

[11] N. Stefan, H.-U. Häring, K. Cusi, Non-alcoholic fatty liver disease: causes, diagnosis, cardiometabolic consequences, and treatment strategies, Lancet Diabetes Endocrinol. 7 (2019) 313–324, https://doi.org/10.1016/S2213-8587(18)30154-2.

[12] L.A. P., K. Hiromi, T.M. R., A.Q. M., G.R. D, Is oil red-O staining and digital image analysis the gold standard for quantifying steatosis in the liver? Hepatology. 51 (2010) 1859, https://doi.org/10.1002/hep.23551.

[13] A. Mehlem, C.E. Hagberg, L. Muhl, U. Eriksson, A. Falkevall, Imaging of neutral lipids by oil red O for analyzing the metabolic status in health and disease, Nat. Protoc. 8 (2013) 1149–1154, https://doi.org/10.1038/nprot.2013.055.

[14] R. Koopman, G. Schaart, M.K. Hesselink, Optimisation of oil red O staining permits combination with immunofluorescence and automated quantification of lipids, Histochem. Cell Biol. 116 (2001) 63–68, https://doi.org/10.1007/s004180100297.

[15] J.L. Ramírez-Zacarías, F. Castro-Muñozledo, W. Kuri-Harcuch, Quantitation of adipose conversion and triglycerides by staining intracytoplasmic lipids with oil red O, Histochemistry 97 (1992) 493–497, https://doi.org/10.1007/BF00316069.

[16] S.D. Fowler, P. Greenspan, Application of Nile red, a fluorescent hydrophobic probe, for the detection of neutral lipid deposits in tissue sections: comparison with oil red O, J. Histochem. Cytochem. 33 (1985) 833–836, https://doi.org/10.1177/33.8.4020099.

[17] D. Sheng, F. Xu, Q. Yu, T. Fang, J. Xia, S. Li, X. Wang, A study of structural differences between liver cancer cells and normal liver cells using FTIR spectroscopy, J. Mol. Struct. 1099 (2015) 18–23, https://doi.org/10.1016/j.molstruc.2015.05.054.

[18] K. Zhang, C. Hao, B. Man, C. Zhang, C. Yang, M. Liu, Q. Peng, C. Chen, Diagnosis of liver cancer based on tissue slice surface enhanced Raman spectroscopy and multivariate analysis, Vib. Spectrosc. 98 (2018) 82–87, https://doi.org/10.1016/j.vibspec.2018.07.010.

[19] M.G. Ramírez-Elías, E.S. Kolosovas-Machuca, D. Kershenobich, C. Guzmán, G. Escobedo, F.J. González, Evaluation of liver fibrosis using Raman spectroscopy and infrared thermography: a pilot study, Photodiagn. Photodyn. Ther. 19 (2017) 278–283, https://doi.org/10.1016/j.pdpdt.2017.07.009.

[20] K.-Z. Liu, A. Man, R.A. Shaw, B. Liang, Z. Xu, Y. Gong, Molecular determination of liver fibrosis by synchrotron infrared microspectroscopy, Biochim. Biophys. Acta Biomembr. 1758 (2006) 960–967, https://doi.org/10.1016/j.bbamem.2006.05.006.

[21] K. Kochan, E. Maslak, C. Krafft, R. Kostogrys, S. Chlopicki, M. Baranska, Raman spectroscopy analysis of lipid droplets content, distribution and saturation level in Non-Alcoholic Fatty Liver Disease in mice, J. Biophotonics 8 (2015) 597–609, https://doi.org/10.1002/jbio.201400077.

[22] Y. Adkins, I.W. Schie, D. Fedor, A. Reddy, S. Nguyen, P. Zhou, D.S. Kelley, J. Wu, A novel mouse model of nonalcoholic steatohepatitis with significant insulin resistance, Lab. Investig. 93 (2013) 1313, https://doi.org/10.1038/labinvest.2013.123.

[23] F. Le Naour, M.-P. Bralet, D. Debois, C. Sandt, C. Guettier, P. Dumas, A. Brunelle, O. Laprévote, Chemical imaging on liver steatosis using synchrotron infrared and ToF-SIMS microspectroscopies, PLoS One 4 (2009) e7408, , https://doi.org/10.1371/journal.pone.0007408.

[24] J. Dybas, K.M. Marzec, M.Z. Pacia, K. Kochan, K. Czamara, K. Chrabaszcz, E. Staniszewska-Slezak, K. Malek, M. Baranska, A. Kaczor, Raman spectroscopy as a sensitive probe of soft tissue composition – imaging of cross-sections of various organs vs. single spectra of tissue homogenates, TrAC Trends Anal. Chem. 85 (2016) 117–127, https://doi.org/10.1016/j.trac.2016.08.014.

[25] S.G. Kazarian, K.L.A. Chan, ATR-FTIR spectroscopic imaging: recent advances and applications to biological systems, Analyst. 138 (2013) 1940–1951, https://doi.org/10.1039/C3AN36865C.

[26] K. Kochan, K. Czamara, K. Majzner, M.Z. Pacia, K. Kochan, A. Kaczor, Raman spectroscopy of lipids: a review, J. Raman Spectrosc. 46 (2014) 4–20, https://doi.org/10.1002/jrs.4607.

[27] I. Dreissig, S. Machill, R. Salzer, C. Krafft, Quantification of brain lipids by FTIR spectroscopy and partial least squares regression, Spectrochim. Acta A Mol. Biomol. Spectrosc. 71 (2009) 2069–2075, https://doi.org/10.1016/j.saa.2008.08.008.

[28] I.W. Schie, L. Nolte, T.L. Pedersen, Z. Smith, J. Wu, I. Yahiatene, J.W. Newman, T. Huser, Direct comparison of fatty acid ratios in single cellular lipid droplets as determined by comparative Raman spectroscopy and gas chromatography, Analyst. 138 (2013) 6662–6670, https://doi.org/10.1039/c3an00970j.

[29] K. Kochan, E. Maslak, S. Chlopicki, M. Baranska, FT-IR imaging for quantitative determination of liver fat content in non-alcoholic fatty liver, Analyst. 140 (2015) 4997–5002, https://doi.org/10.1039/C5AN00737B.

[30] K.C. Hewitt, J. Ghassemi Rad, H.C. McGregor, E. Brouwers, H. Sapp, M.A. Short, S.B. Fashir, H. Zeng, I.P. Alwayn, Accurate assessment of liver steatosis in animal models using a high throughput Raman fiber optic probe, Analyst. 140 (2015) 6602–6609, https://doi.org/10.1039/C5AN01080B.

[31] M.Z. Pacia, K. Czamara, M. Zebala, E. Kus, S. Chlopicki, A. Kaczor, Rapid diagnostics of liver steatosis by Raman spectroscopy via fiber optic probe: a pilot study, Analyst. 143 (2018) 4723–4731, https://doi.org/10.1039/C8AN00289D.

[32] T.T. Le, A. Ziemba, Y. Urasaki, S. Brotman, G. Pizzorno, Label-free evaluation of hepatic microvesicular steatosis with multimodal coherent anti-stokes Raman scattering microscopy, PLoS One 7 (2012) e51092, , https://doi.org/10.1371/journal.pone.0051092.

[33] Y. Urasaki, C. Zhang, J.-X. Cheng, T.T. Le, Quantitative assessment of liver steatosis and affected pathways with molecular imaging and proteomic profiling, Sci. Rep. 8 (2018) 3606, https://doi.org/10.1038/s41598-018-22082-6.

[34] Y. Yu, P.V. Ramachandran, M.C. Wang, Shedding new light on lipid functions with CARS and SRS microscopy, Biochim. Biophys. Acta Mol. Cell Biol. Lipids 1841 (2014) 1120–1129, https://doi.org/10.1016/j.bbalip.2014.02.003.

[35] A. Derenne, O. Vandersleyen, E. Goormaghtigh, Lipid quantification method using FTIR spectroscopy applied on cancer cell extracts, Biochim. Biophys. Acta Mol. Cell Biol. Lipids 1841 (2014) 1200–1209, https://doi.org/10.1016/j.bbalip.2013.10.010.

[36] V. Esposito Vinzi, W.W. Chin, J. Henseler, H. Wang (Eds.), Handbook of Partial Least Squares, Springer Berlin Heidelberg, Berlin, Heidelberg, 2010, , https://doi.org/10.1007/978-3-540-32827-8.

[37] T.K. Dijkstra, Part I: methods of partial least squares, in: V. Esposito Vinzi, W.W. Chin, J. Henseler, H. Wang (Eds.), Handb. Partial Least Squares, Springer Berlin Heidelberg, Berlin, Heidelberg, 2010, pp. 23–46, , https://doi.org/10.1007/978-3-540-32827-8.

[38] M. Haenlein, A.M. Kaplan, A beginner's guide to partial least squares analysis, Underst. Stat. 3 (2004) 283–297, https://doi.org/10.1207/s15328031us0304_4.

[39] L.O. Schwen, A. Homeyer, M. Schwier, U. Dahmen, O. Dirsch, A. Schenk, L. Kuepfer, T. Preusser, A. Schenk, Zonated quantification of steatosis in an entire mouse liver, Comput. Biol. Med. 73 (2016) 108–118, https://doi.org/10.1016/j.compbiomed.2016.04.004.